

The Multi-Body Dynamic Analysis of High-Mobility Tracked Vehicle on Different Ground Friction Conditions

Jung-Kuang Cheng* and Yunn-Lin Hwang**

Keywords: Multi-body dynamic analysis, High-mobility, Tracked vehicle, Ground friction conditions.

ABSTRACT

Several modelling methods had recently been developed for the dynamic analysis of tracked vehicles. These methods are used demonstrate the significant force effects of the interaction between the track links and vehicle components. There are two major difficulties encountered in developing the compliant track models discussed in this paper. The first problem is due to the integration step size must be kept small in order to maintain the numerical stability of the solution. This solution includes high oscillatory signals resulting from the impulsive contact force and the use of stiff compliant elements to present the joints between the track links. The characteristics of the compliant elements use in this paper to describe the track joints were measured experimentally. A numerical method having a relatively large stability region is employed in order to maintain the solution accuracy, and a variable step size integration algorithm is used in order to improve the efficiency. The second difficulty encountered in this paper is due to the large number of the system equation of motion of three-dimensional multi-body high-mobility tracked vehicles model. The dimensionality problem is solved by decoupling the equations of motion of chassis and track subsystems. Recursive method is used to obtain a minimum set of equations for the chassis subsystem. Several ground friction simulation scenarios including an accelerated motion, high-speed motion, braking, and turning motion of high-mobility vehicle are tested and verified in order to demonstrate the effectiveness and validity of the methods proposed in this paper.

Paper Received May, 2019. Revised November, 2019. Accepted December, 2019. Author for Correspondence: Yunn-Lin Hwang.

* *Ph.D. Student, Institute of Mechanical and Electro-Mechanical Engineering, National Formosa University, Yunlin, Taiwan 63201, ROC.*

** *Professor, Department of Mechanical Design Engineering, National Formosa University, Yunlin, Taiwan 63201, ROC.*

INTRODUCTION

High-speed, high-mobility tracked vehicles are subjected to impulsive dynamic loads resulting from the interaction of the track chains with the vehicle components and the ground. These dynamic loads can have an adverse effect on the vehicle performance and can cause high stress levels that limit the operational life of the vehicle components. For this reason, high-speed, high-mobility tracked vehicles have sophisticated suspension systems, a more elaborate and detailed design of the links of the track chains, and improved vibration characteristics that allow the vehicle to perform efficiently in hostile operating environments. Galaitsis (1984) demonstrated that the predicted dynamic track tension and suspension loads in a high-speed tracked vehicle developed by an analytical method are useful in evaluating the dynamic characteristics of the tracked vehicle components. Nakanishi and Shabana (1994) developed a two-dimensional contact force model for planar analysis of multi-body tracked vehicle systems. Ma and Perkins (2006) presented a track-wheel-terrain interaction model which can be used as a "force" super-element in a multibody dynamics code for dynamic simulation of tracked vehicles. This model employs a nonlinear finite element representation for the track segment that is in contact with the terrain and roadwheels, which can be used to simulate two different track systems, namely a continuous rubber band track and a multi-pitched metallic track, provided the finite element mesh in the track model is properly defined. The new track model accounts for the tension variations along the track (due to the non-uniformly distributed normal pressure and traction), track extensibility, and geometrically large (nonlinear) track deflections. Chu *et al.* (2009) had done a detailed investigation which is performed to simulate the flow field in the air cleaner of an all-terrain vehicle (ATV) including theoretical simulation and experimental verification. Choi *et al.* (1998) presented a large scaled multi-body dynamic model of construction tracked vehicle in which the track is assumed to consist of track links connected by single degree of freedom pin joints. Tsai and Chen (2011) developed a 9 degree-of-freedom (DOF)

mathematical model to analyze the dynamic behavior of high-speed railway vehicle truck running on curved tracks with worn and eccentric wheelset. The Kalker's linear creep theory is applied to investigate the contact forces between the wheels and rail. The hunting (critical) speeds, the effects of primary suspension stiffness, the flange contact force and the angle of attack with worn wheelset are investigated. Tong *et al.* (2013) proposed a new hysteresis contact force model to simulate the vibration characteristics with road profile excitation. The dynamic characteristics, period doubling bifurcation, hardening type nonlinearity and the coexisting of periodic solutions are studied numerically with bifurcation map, phase portraits and basin of attractor. The cell mapping method is introduced to study the global characteristics of the quarter car vibrations. Liang *et al.* (2018) describes how to design and analyze the suspension system. According to the tire characteristics, geometric parameters of the transverse arms, elastic elements and damping elements are firstly determined. Then the dynamic model of the vehicle suspension system is established. Finally, the kinematic and dynamic analysis are carried out to verify the effectiveness of the suspension system design.

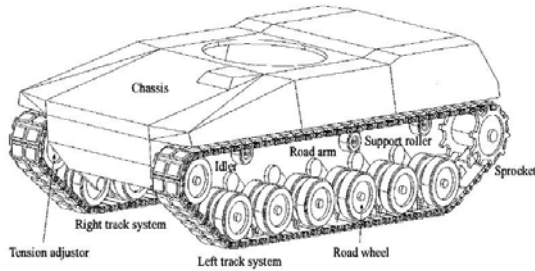


Fig. 1. High mobility tracked vehicle

HIGH-MOBILITY TRACKED VEHICLE

As shown in Figure 1, the high-speed, high-mobility tracked vehicle model used in this investigation is described. The three-dimensional model, which is shown in Figure 1, represents the third generation of a military vehicle weighing approximately 50 tons and can be driven at a speed higher than 60 km/h. The vehicle consists of a chassis and two track subsystems. The chassis subsystem includes a chassis, sprockets, support rollers, idlers, road arms, road wheels and the suspension units. The sprockets, support rollers, and road arms are connected to the chassis by revolute joints. The suspension unit includes a Hydro-pneumatic Suspension Unit (HSU) (Maclaurin, 1983) and torsion bar that are modelled as force elements whose compliance characteristics are evaluated using analytical and empirical methods. The

spring torque of the HSU systems can be written as Eq.(1)

$$T_{HSU} = PAL_1 \quad (1)$$

where P is the gas pressure, A is the area of piston, L_1 is the distance shown in the Figure 2.

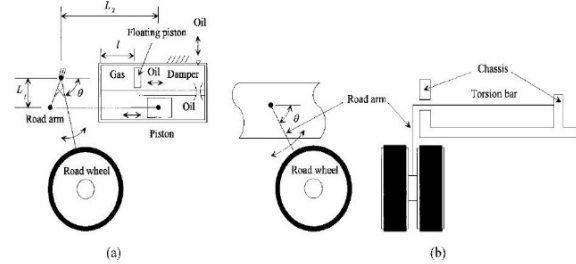


Fig. 2. Schematic diagram of spring-damper suspension units: (a)Hydro pneumatic suspension unit; (b)Torsion bar systems

The pressure P in the gas chamber of HSU system with respect to rotation angle of a road arm is defined as Eq.(2):

$$M_i^c = B^T MB, \quad Q_i^c = B^T (Q - \dot{B}q_i^r)$$

$$P = P_i \left[\frac{l_i}{l_s + (L_{2i} - L_2)} \right]^\gamma \quad (2)$$

where P_i , l_i , and l_{2i} are the initial pressure and distances when the road arm is in its initial configuration, γ is a constant which is equal to 1.4, and l_2 is the distance as shown in Figure 2. The distance l_s can be adjusted by charging or discharging oil into the oil chamber. Each track subsystem is modeled as a series of bodies connected by rubber bushings around the link pins which are inserted into a shoe plate with some radial pressure in order to reduce the non-linear effect of the rubber. When the vehicle runs over rough surfaces, the track chains are subjected to extremely high impulsive contact forces as the result of their interaction with the vehicle components such as road wheels, idlers, and sprocket teeth, as well as the ground. The rubber bushings and double pins tend to reduce the high impulsive contact forces by providing cushion and reducing the relative angle between the track links. About 10 percent of the vehicle weight is given as the pre-tension for the track to prevent frequent separations of the track when the vehicle runs at a high speed. About 14 degrees of a pre-torsion is also provided in order to reduce the fluctuation of the torque in the rubber bushing when the track links contact the sprocket and idler.

KINEMATIC EQUATION OF MOTION

Recursive kinematic equations of tracked vehicles were presented by Lee *et al.* (1998), who showed that the relationship between the absolute Cartesian velocities of the chassis components can be expressed in terms of the independent joint velocities as Eq.(3):

$$\dot{q} = B\dot{q}_i^r \quad (3)$$

Where \dot{q} , B and \dot{q}_i^r are relative independent coordinate, velocity transformation matrix, and Cartesian velocities of the chassis subsystem, respectively. The equations of motion of the chassis that employs the velocity transformation defined in the preceding equations are given as Eq.(4)

$$B^T M B \ddot{q}_i^r = B^T (Q - \dot{B} \dot{q}_i^r) \quad (4)$$

where M is the mass matrix, and Q is the generalized external force vector of the chassis subsystems. Since there is no kinematic coupling between the chassis subsystem and the track subsystems, the equation of motion of the chassis subsystem can be obtained using the preceding equation as follows:

$$M_i^c \ddot{q}_i^r = Q_i^c \quad (5)$$

where M^c , q^r and Q^c denote the mass matrix; and the generalized coordinate and force vectors for the chassis subsystem.

For the track systems, the equations of motion can be written as:

$$M^t \ddot{q}^t = Q^t \quad (6)$$

Where M^t , q^t and Q^t denote the mass matrix; and the generalized coordinate and force vectors for the track subsystem. Consequently, the accelerations of the chassis and the track links can be obtained by solving Eqs. (5) and (6).

SINGULAR CONFIGURATIONS

In order to demonstrate some of the difficulties encountered when the independent coordinates are not properly selected, we consider the closed kinematic chain shown in Figure 3. Such a closed kinematic chain that consists of n_{ab} links connected by revolute joints has n_b degrees of freedom. In order to define the chain configuration in the global coordinate system, at least two translational Cartesian coordinates must be

selected as degrees of freedom, as shown in Fig. 3. The other remaining degrees of freedom can be selected as rotation angles, and hence there are two rotational coordinates for two links that must be treated as dependent coordinates. The dependent rotational coordinates can be expressed in terms of the independent angles using the loop-closure equations

$$\left\{ \sum_{i=1}^{n_b} l \cos \theta^i \right\} + l \cos \theta^j + l \cos \theta^k = 0 \quad (7)$$

$$\left\{ \sum_{i=1}^{n_b} l \sin \theta^i \right\} + l \sin \theta^j + l \sin \theta^k = 0 \quad (8)$$

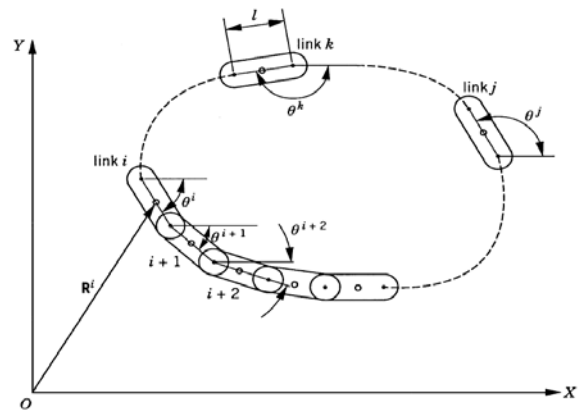


Fig. 3. Singular configurations

where n_b is the total number of the links, θ^j and θ^k are the dependent rotation angles of the links j and k , and l is the length of the link. For simplicity, we assumed here that all the links are of equal length. The preceding two equations can be written as Eqs. (9) and (10):

$$l \cos \theta^j + l \cos \theta^k = A \quad (9)$$

$$l \sin \theta^j + l \sin \theta^k = B \quad (10)$$

Where A and B can be expressed as Eqs. (11) and (12):

$$A = - \sum_{i=1}^{n_b} l \cos \theta^i \quad (11)$$

$$B = - \sum_{i=1}^{n_b} l \sin \theta^i \quad (12)$$

By differentiating the resulting loop-closure equations with respect to time, one obtains

$$\left\{ \sum_{i=1}^{n_b} l \dot{\theta}^i \sin \theta^i \right\} + l \dot{\theta}^j \sin \theta^j + l \dot{\theta}^k \sin \theta^k = 0 \quad (13)$$

$$\left\{ \sum_{i=1}^{n_b} l \dot{\theta}^i \cos \theta^i \right\} + l \dot{\theta}^j \cos \theta^j + l \dot{\theta}^k \cos \theta^k = 0 \quad (14)$$

Equations (13) and (14) can be rewritten as Eqs. (15) and (16):

$$l \dot{\theta}^j \sin \theta^j + l \dot{\theta}^k \sin \theta^k = -A_d \quad (15)$$

$$l \dot{\theta}^j \cos \theta^j + l \dot{\theta}^k \cos \theta^k = -B_d \quad (16)$$

Where A_d and B_d can be expressed as Eqs. (17) and (18):

$$A_d = \frac{dA}{dt} = \sum_{i=1}^{n_b} l \dot{\theta}^i \sin \theta^i \quad (17)$$

$$B_d = \frac{dB}{dt} = \sum_{i=1}^{n_b} l \dot{\theta}^i \cos \theta^i \quad (18)$$

It follows that:

$$\begin{bmatrix} l \sin \theta^j & l \sin \theta^k \\ l \cos \theta^j & l \cos \theta^k \end{bmatrix} \begin{bmatrix} \dot{\theta}^j \\ \dot{\theta}^k \end{bmatrix} = - \begin{bmatrix} A_d \\ B_d \end{bmatrix} \quad (19)$$

This system of Eq.(19) can be solved for $\dot{\theta}^j$ and $\dot{\theta}^k$ as Eq.(20):

$$\begin{bmatrix} \dot{\theta}^j \\ \dot{\theta}^k \end{bmatrix} = \frac{-1}{l \sin(\theta^j - \theta^k)} \begin{bmatrix} A_d \cos \theta^k - B_d \sin \theta^k \\ -A_d \cos \theta^j + B_d \sin \theta^j \end{bmatrix} \quad (20)$$

It is clear from this equation that singularities will be encountered when $\theta^j - \theta^k$ is close to or equal to 0 or π . In these situations, an alternate set of independent coordinates must be used; otherwise, a small error in the independent variables will lead to a very large error in the dependent variables. It is clear from the closed-chain example that if the set of independent coordinates is defined only once at the beginning of the simulation, numerical difficulties may be encountered when the system configuration changes. If the error in the dependent coordinates becomes large, the number of the Newton-Raphson iterations required to solve the nonlinear kinematic constraint equations will significantly increase. Furthermore, the numerical errors in the dependent coordinates may lead to significant changes in the forces and system inertia, which, in turn, make the dynamic equations appear as being stiff, thereby forcing the numerical integration method to select a smaller step size.

CONTACT FORCE

A. Interaction between track and road wheel, idler, and support roller.

- A.1 The first possibility occurs when a track link and one wheel of the roller are in contact. In this case, a concentrated contact force is used at the center of the contact surface of the wheel. The contact force acting on the link is assumed to be equal in magnitude and opposite in direction to the force acting on the roller.
- A.2 The second possibility occurs when both wheels of the rollers are in contact with the track link. In this case, two concentrated contact forces are applied to the roller and the track link.
- A.3 The third and fourth possibilities occurs when either one wheel and both wheels are in contact with the edges of track link. In such a case, one or two concentrated contact forces are applied to the wheel and the edge of the track link.

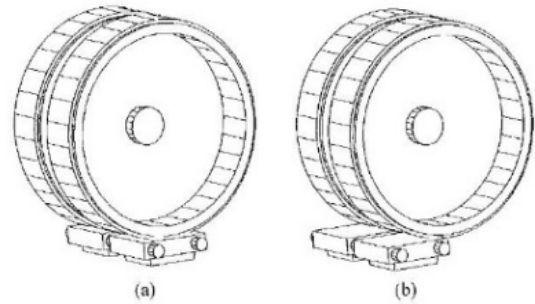


Fig. 4. Track link and wheel interaction: (a)Inner surface; (b)Edge contact

B. Track center guide and road wheel interactions.

- B.1 The first possibility is the case in which the right-side plate of the wheel is in contact with the left-side wall of the track center guide.
- B.3 The second and third possibility occurs when one bottom surface of wheel and the top surface of track center guide are in contact. In these three contact cases, a concentrated contact force is introduced at the contact surface of the road wheels, and that contact force is equal in magnitude and opposite in direction to the force acting on the track link.
- B.4 The fourth possibility occurs when the two road wheels are not in contact with the track center guide.

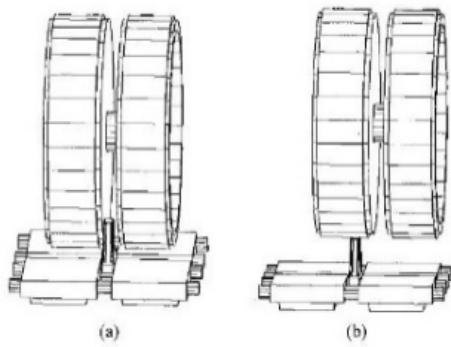


Fig. 5. Center guide and wheel interactions:
(a)Side wall contact; (b)Top surface contact

C. Interaction between the sprocket teeth and track link pins.

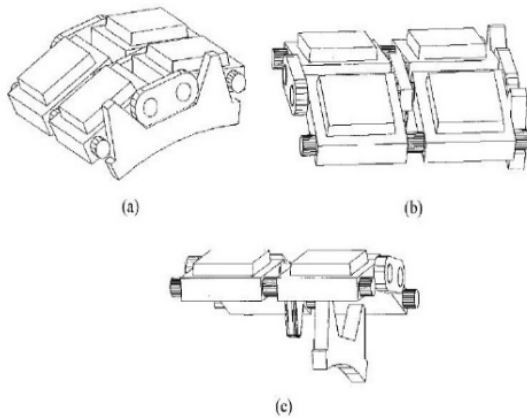


Fig. 6. Sprocket tooth and track interaction:
(a)Sprocket teeth and connector contact;
(b)Teeth side wall and link side wall contact;
(c)Teeth top surface and link inner surface.

In this investigation, five tooth surfaces are used to present the spatial contact between the sprocket teeth and the track link pins. During the course of engagement between the sprocket teeth and the track links, several sprocket teeth can be in contact with several track link pins, as show in Figure 6. The sprocket used in this investigation has ten teeth, and each tooth has five contact surfaces. These surfaces are the top, the left, the right, front, and back surfaces. A Cartesian coordinate system has a constant orientation with respect to the sprocket coordinate system. Therefore, the orientation of a surface coordinate system can be defined in the global system using three coordinate transformation matrices; two of them are constant and the third is time dependent rotation matrix of the sprocket. Using the coordinate transformations and the absolute Cartesian coordinates of the origin of the sprocket coordinate system, the location and orientation of each tooth surface can be defined in the global coordinate system.

Using the track link coordinate system, the global position vector of the center of the track link pin can be defined. This vector and the global coordinates of the tooth surfaces can be used to determine the position of the track link pins with respect to the sprocket teeth. The relative position of the track link pins, with respect to the sprocket to the sprocket teeth can be used to develop a computer algorithm that determines whether or not the track link pin is in contact with one of surfaces of the sprocket teeth. The interactions between the track link pins and the sprocket base circle are also considered in this investigation. To the end, the distance between the center of the track link pin and the center of sprocket is monitored. When this distance is less than the sum of the pin radius and the sprocket base circle radius, contact is assumed and a concentrated force is applied to the sprocket and the track link pin.

D. Ground and track shoe interactions.

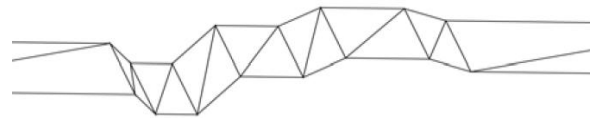


Fig. 7. Terrain representation (Obstacle course)

The track link used in this investigation has a single or double shoe plate. Therefore, there are one or two surfaces on each track link that can come into contact with the ground. The global position vectors that define the location of points on the shoe plates are expressed in terms of the generalized coordinates of the track links and are used to predict whether or not the track link is in contact with the ground. In this investigation, contact forces are applied at selected six points on the track link shoe when it comes into contact with the ground. The normal force components are used with the coefficient of friction to define the tangential friction forces.

NUMERICAL MODEL

In this investigation, a simple numerical tank model is used as shown in Table 1. For the ground conditions, the first case is that the tank moved on smooth surface as shown in Figure 8 and the second case is that the tank moved on rough surface as shown in Figure 9.

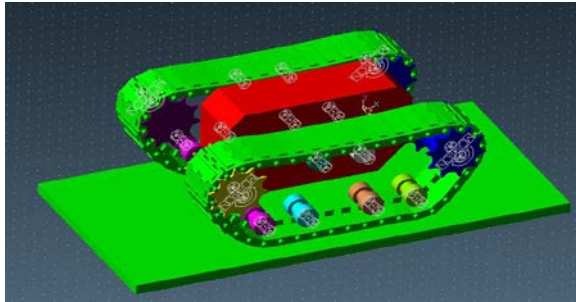


Fig. 8. Tank moved on smooth surface

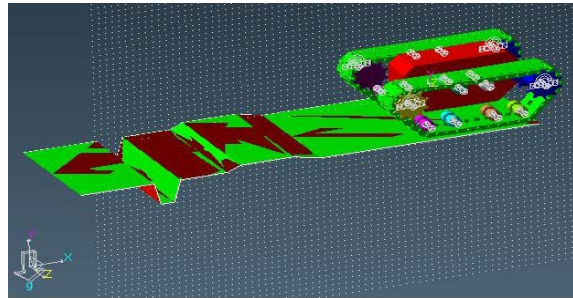


Fig. 9. Tank moved on rough surface

Table 1
Numerical Tank Model Parameters

Parametric table		
Sprocket	Sprocket Carrier Radius (Ri)	160 mm
	Sprocket Carrier Width (Wi)	480 mm
	Sprocket Total Width (Wo)	528 mm
	Number of Teeth	10
	Dedendum Circle Radius (Rd)	216 mm
	Base Circle Radius (Rib)	226.712 mm
	Pitch Circle Radius (Rp)	249.744 mm
	Addendum Circle Radius (Ra)	281.92 mm
	Pin Circle Radius	23.17 mm
	Loop Radius	249.744 mm
	Mass	1 Kg
Double wheel	Hub Radius (Ri)	67 mm
	Wheel Radius (Ro)	100
	Hub Width (Wi)	100
	Total Width (Wo)	300 mm
	Mass	60.4 Kg
Track link	Link Body left Length (Ll)	96 mm
	Link Body Right Length (Lr)	96 mm
	Link Body Upper Height (Hu)	40.12 mm
	Link Body Lower Height (Hb)	40.12 mm
	Link Body width (Wb)	464 mm
	Link Body Connector Length (Lt)	32 mm
	Pin Length (Lp)	544 mm
	Pin Radius (Rp)	21.76 mm
	Centerguide Length (Lc)	80 mm
	Centerguide Thickness (Tc)	34.4 mm
	Mass	54.2 Kg

In the rough surface case, the total force of each track link is shown in Figure 10. The force of double wheel on X-direction is shown in Figure 11. The force of double wheel on Y-direction is shown in Figure 12.

The total magnitude of the track link's position is shown in Figure 13. The total magnitude of the track link's velocity is shown in Figure 14. The total magnitude of the track link's acceleration is shown in Figure 15.

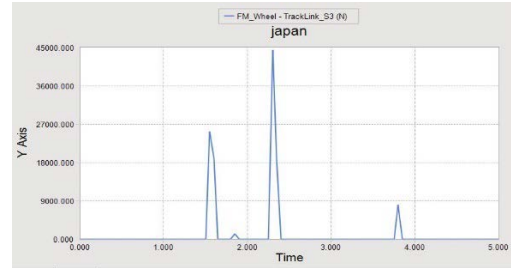


Fig. 10. Total force of each track link

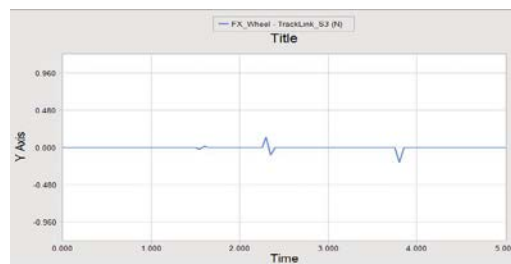


Fig. 11. Force of double wheel on X-direction

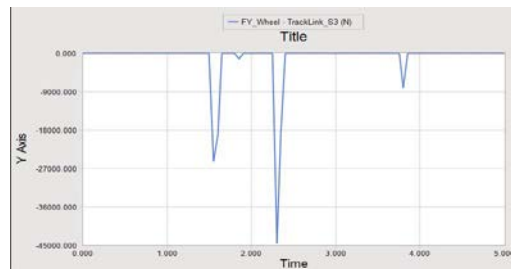


Fig. 12. Force of double wheel on Y-direction

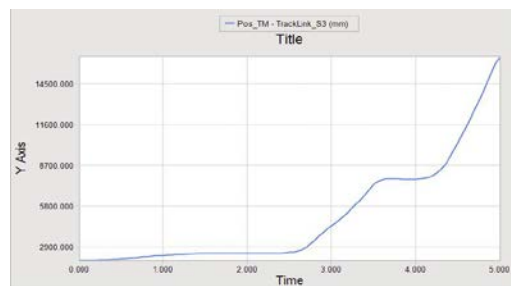


Fig. 13. Total magnitude of track link's position

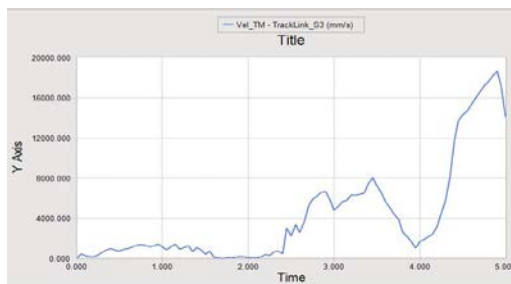


Fig. 14. Total magnitude of track link's velocity

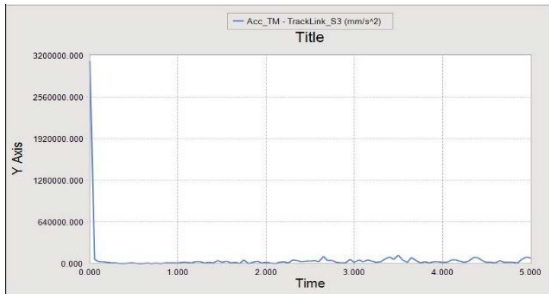


Fig. 15. Total magnitude of track link's acceleration

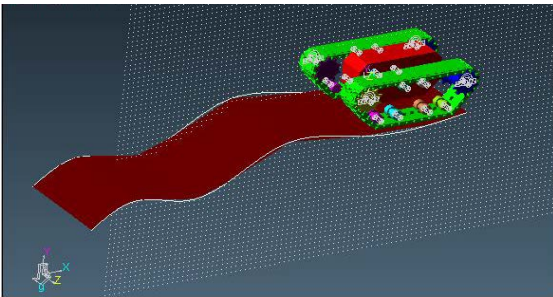


Fig. 16. The slope road surface

In the slope road surface case as shown in Figure 16, the total force of each track link is shown in Figure 17. The force of double wheel on y-direction is shown in Figure 18. The total magnitude of the track link's position is shown in Figure 19. The total magnitude of the track link's velocity is shown in Figure 20. The total magnitude of the track link's acceleration is shown in Figure 21.

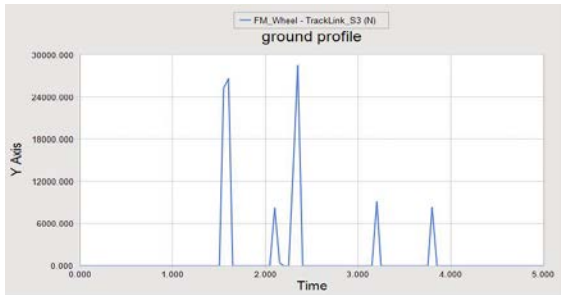


Fig. 17. Total force of each track link

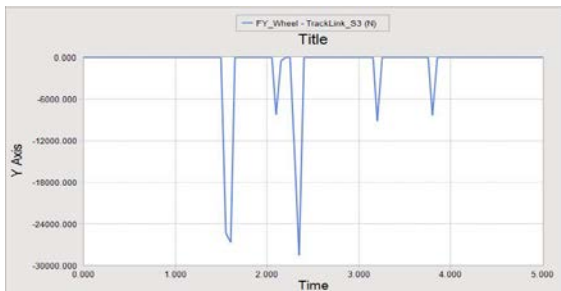


Fig. 18. Force of double wheel on Y-direction

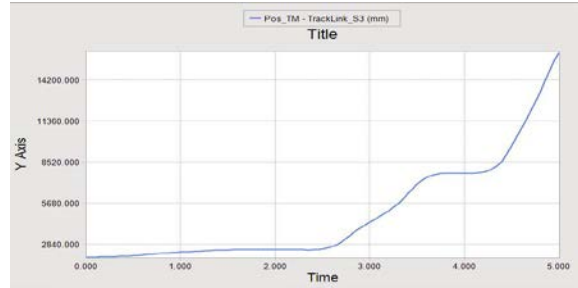


Fig. 19. Total magnitude of track link's position

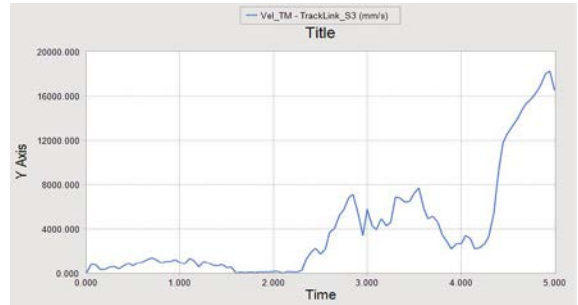


Fig. 20. Total magnitude of track link's velocity

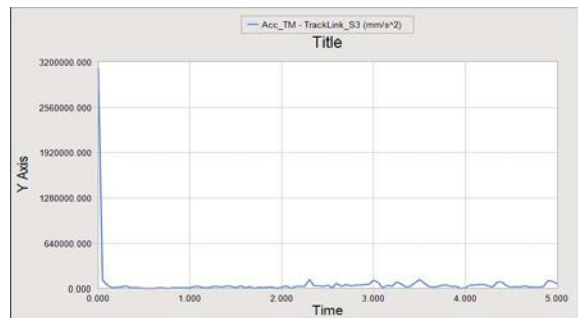


Fig. 21. Total magnitude of track link's acceleration

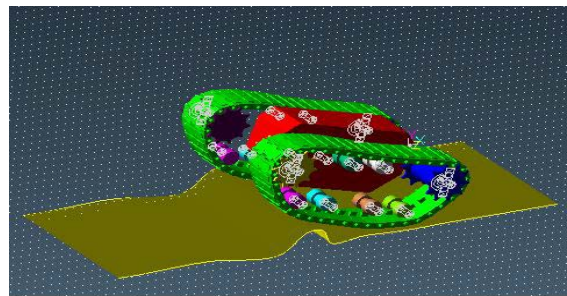


Fig. 22. The obstacle road surface

In the obstacle road surface case as shown in Figure 22, the total force of each track link is shown in Figure 23. The force of double wheel on X-direction is shown in Figure 24. The force of double wheel on Y-direction is shown in Figure 25.

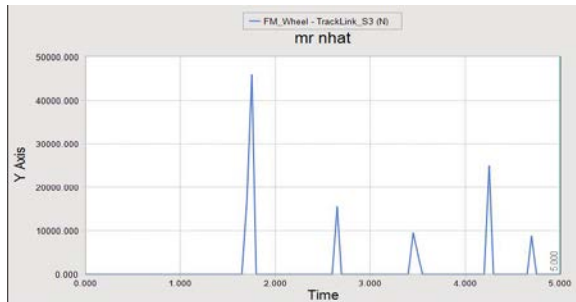


Fig. 23. Total force of each track link

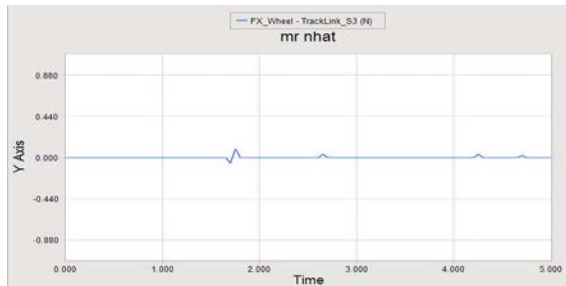


Fig. 24. Force of double wheel on X-direction

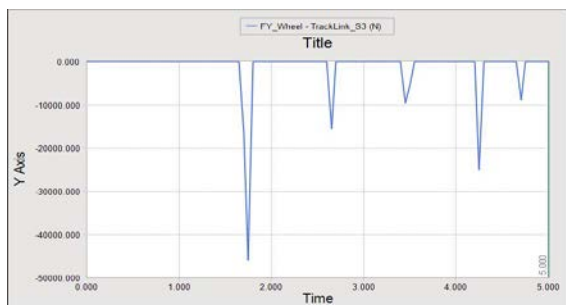


Fig. 25. Force of double wheel on Y-direction

CONCLUSION AND SUMMARY

Compliant force elements are used to define the connectivity between the links of the track chains instead of an ideal pin joint. Two track link models are considered in this study. These are the single pin and double pin track models. In the single pin track model, only one pin is used to connect two track links in the chain. In the double pin track model, two pins are used with a connector element to connect two links of the track chain. Rubber bushings are used between the track links and the pins. The stiffness and damping characteristics of the contact forces are obtained using experimental testing. Consequently, we use RecurDyn software to simulate these high-mobility tracked vehicle CAE models. By using this software, we can investigate some factors such as position, velocity, acceleration and dynamic force analysis.

ACKNOWLEDGEMENT

This research work is supported by Ministry of

Science and Technology of Taiwan under the grant contracts MOST 107-2221-E-150-011 and MOST 107-2622-E-150-006-CC3.

REFERENCES

- Galatsis., A. G., "TRAXION: A Model for predicting dynamic track loads in military vehicles," *Journal of Vibration Acoustics Stress and Reliability in Design*, Vol. 106, pp. 286-291. (1984)
- Nakanishi, T. and Shabana, A. A., "Contact forces in the nonlinear dynamic analysis of tracked vehicles," *Int. Journal for Numerical Methods in Engineering*, Vol. 37, pp. 1251-1275. (1994)
- Ma, Zheng-Dong, Perkins, N. C., "A Super-Element of Track-Wheel-Terrain Interaction for Dynamic Simulation of Tracked Vehicles," *Int. Journal of Multibody System Dynamics*, Vol. 15, pp. 351-372. (2006)
- Chu, Li-Ming, Chang, Min-Hsing, Chen, Jiann-Lin and Lai, Jin-Yuan, "Simulation and experimental measurement of flow field within an air cleaner of all-terrain vehicle," *Journal of the Chinese Society of Mechanical Engineers*, Vol. 30, No. 2, pp. 143-150. (2009)
- Choi, J. H., Lee, H. C., Shabana, A. A., "Spatial Dynamics of Multibody Tracked Vehicles Part I: Spatial Equation of Motion," *Vehicle System Dynamics: Int. Journal of Vehicle Mechanics and Mobility*, Volume 29, Issue 1, pp. 27-49. (1998)
- Tsai, Meng-Shiun, Chen, Sue-Ker, "Analysis of High-Speed Railway Vehicle Trucks with Worn and Eccentric Wheelset Moving on Curved Tracks," *Journal of the Chinese Society of Mechanical Engineers*, Vol. 32, No. 4, pp. 331-340. (2011)
- Tong, Lin-jun, Yang, Yue, Huang, Hui-yuan, Li, Qiue, Chen, Feng and Li, Xiong-bing, "Bifurcation Analysis of Nonlinear Vehicle System under Road Excitation," *Journal of the Chinese Society of Mechanical Engineers*, Vol. 34, No. 4, pp. 313-320. (2013)
- Liang, Zhi-Qiang, Liu, Xin-Tian, Zuo, He, Li, and Wang, Yan-Song, "Design and Analysis of Suspension System Based on Tire Characteristics," *Journal of the Chinese Society of Mechanical Engineers*, Vol. 39, No. 6, pp. 599-608. (2018)
- Maclaurin, B., "Progress in British tracked vehicle suspension systems," *Society of Automotive Engineers*. (1983)
- Lee, H. C., Choi, J. H. and Shabana, A. A., "Spatial Dynamics of Multibody Tracked Vehicles Part II: Contact Forces and Simulation Results," *Vehicle System Dynamics: Int. Journal of Vehicle Mechanics and Mobility*, Volume 29, Issue 2, pp. 113-137. (1998)

高機動履帶車輛在不同地面摩擦條件下的多體動力學分析

鄭榮光

國立虎尾科技大學機械與機電工程研究所博士候選人

黃運琳

國立虎尾科技大學機械設計工程系教授

摘要

本文介紹了近年來開發的幾種運用於履帶車輛動態分析的建模方法。這些方法應用於同時考慮履帶鏈節和車輛部件之間的相互作用的顯著的力效應。在研究開發本文所討論的順應軌道模型時遇到兩個主要困難點。第一個必須克服的問題點乃是由於集成步長必須保持較小以保持數值解的數值穩定性。該解決方案包括由脈衝接觸力產生的高振盪信號和使用剛性柔順元件來呈現履帶鏈節之間的接頭。在本研究中使用柔順元件的特徵來描述軌道接頭是通過實驗測量的。採用具有相對大的穩定區域的數值方法以保持求解精度，並且使用可變步長積分算法以提高效率。本研究遇到的第二個困難克服點是由於三維多體高機動履帶車輛模型的大量系統運動方程組。通過求解底盤和軌道子系統的運動方程來解決維數問題。遞歸方法運用於獲得機械子系統的最小方程組。為了證明本研究中提出的方法的有效性和正確性，對於包括高移動性車輛的加速運動，高速運動，制動和轉向運動在內的幾種模擬不同接觸地面摩擦條件下進行測試與驗證。